Paleoceanography and Paleoclimatology

Supporting Information for

Extreme Planktic Foraminiferal Dwarfism Across the ETM2 in the Tethys Realm in response to warming

R. D'Onofrio[1,2], R. Barrett[3], D. N. Schmidt[3], E. Fornaciari[4], L. Giusberti[4], G. Frijia[1], T. Adatte[5], N. Sabatino[6], A. Monsuru[3], V. Brombin[1], and V. Luciani[1]

[1]Dipartimento di Fisica e Scienze della Terra, Università di Ferrara, Ferrara, Italy; [2]Istituto di Scienze Marine (ISMAR), CNR, Venezia, Italy; [3]School of Earth Sciences, University of Bristol, Bristol, U.K.; [4]Dipartimento di Geoscienze, Università di Padova, Padova, Italy; [5]GEOPOLIS, ISTE, Lausanne University, Lausanne, Switzerland; [6]Istituto per lo studio degli impatti Antropici e Sostenibilità in ambiente marino (IAS), CNR, Palermo, Italy

Contents of this file

1. Supplementary Text: Introduction, Text S1
2. Figures S1 to S4
3. Titles of dataset tables that are available in .xlsx and html format to the Pangea repository by the DOI of the following dataset publication D'Onofrio, et al. (2024): Extreme Planktic Foraminiferal Dwarfism Across the ETM2 in the Tethys Realm in response to warming [dataset bundled publication]. PANGAEA, https://doi.org/10.1594/PANGAEA.967574

1. Supplementary Text

Introduction

The supporting information gives details on how and with which elements, mercury can be fixed into sediment (Text S1). We clarify that, to evaluate the volcanic origin of the Hg anomalies present in the Terche and Madeago sections, the relations between Hg and TOC, clay minerals (phyllosilicates) and pyrite have been carefully evaluated though the record of trace elements (TEs) data obtained by XRF. The Hg and TEs concentrations normalized against Rb (Figure S1) and Th (Figure S2) for both sections allow to assume that Hg enrichments are from volcanic origin and not directly related detrital input fluctuations or silicate dilution.

In the binary plots of Figures S3 we show that dissolution indices based on foraminifera and calcareous nannofossil versus each other and the $CaCO_3$ content at the Madeago (in blu) and Terche (in red) sections do not show correlation with $CaCO_3$. The low variations recorded by our whole set of dissolution proxies indicate that dissolution at the ETM2 did not significantly impacted the original signal of planktic foraminifera and calcareous nannofossil assemblages.

Text S1. How and with which elements, mercury can be fixed into sediment?

Mercury (Hg) can be preferentially adsorbed into organic matter, hydrous iron oxides and pyrites, and/or clay minerals (Sanei et al., 2012; Sial et al., 2013; Percival et al., 2015; Font et al., 2016; Grasby et al., 2013, 2019; Them et al., 2019; Shen et al., 2019). Organic matter is generally the main Hg scavenging phase, mainly in the form of organic–Hg complexes (Ravichandran, 2004). Clay soils also have a strong ability to retain Hg species and can also adsorb HgII due to their high surface area and surface charges (Farrah and Pickering, 1978, Kongchum et al, 2011), providing significant terrestrial Hg contents to shallow-marine sediments (Them et al., 2019). Sulfide minerals can be the main host for Hg in euxinic facies because of their high affinity of Hg for sulfide (Bower et al., 2008). In such facies, aqueous HgII can be removed to the sediment by formation of HgS and adsorption onto iron sulfides (Benoit et al., 1999; Bouffard and Amyot, 2009). Sulfide minerals such as pyrite (FeS2), pyrrhotite (Fe1−xS), and mackinawite (FeS) may therefore host large amounts of Hg in some natural settings (Wolfenden et al., 2005; Han et al., 2014). The two latter minerals are generally not significantly present in sediments and will be therefore not discussed herein. Significant correlations between Hg concentrations and Fe and Al oxides/hydroxydes and soil organic matter have been thus observed by many authors (e.g. Schuster et al., 2002, Montoya et al, 2019).

Mercury has a strong affinity for organic matter (OM) in both marine and freshwater environments, reflected by significant Hg enrichments in organic-rich deposits in comparison to other sediments (Sanei et al., 2012). In the aquatic system a number of processes may affect dissolved Hg2+. For example, in oxygen depleted water methyl-mercury (MeHg) is generated by anaerobic microorganisms, which include sulfate-reducing bacteria, iron-reducing bacteria, and methanogens (Wood et al., 1968; Hamelin et al., 2011; Lin et al., 2012, Gascon-Diez et al, 2016). Consequently, bioaccumulation of MeHg leads to the formation of organo-mercury complexes (Hg-OM), which may amplify Hg concentrations recorded in OM-rich sediments. Changes in OM deposition may therefore influence the rates of Hg drawdown (Outridge et al., 2007; Gehrke et al., 2009; Stern et al., 2009), even if Hg sequestration is not directly related to the degree of anoxia. A significative correlation has been observed between Hg and organic carbon enrichments (Outridge et al., 2007; Grasby et al., 2013). Hg concentrations are therefore normalized against total organic carbon (TOC) contents in order to ensure that Hg enrichments are not directly related increased OM accumulation and /or preservation (Percival et al., 2015). A significant correlation between Hg/TOC ratios and the raw Hg data indicate that the Hg enrichments are not related to changes in OM deposition alone (Grasby et al., 2013; Sanei et al., 2012; Font et al., 2016; Grasby, 2019). In this context, the effect of OM degradation on Hg sequestration during burial and exposure remains poorly investigated, and it is yet unclear to which extent the OM preservation history may affect Hg contents in ancient sediments (Charbonnier et al, 2022).

In both Madeago and Terche sections, TOC contents are very low (Madeago :< 0.32 wt%, mean value: 0.10wt% , Terche: <0.14wt%, mean value 0.07 wt%) (Figure S1, S2) Hg cannot be therefore normalized by TOC (Grasby, 2019).

Cited references in the main text

2. Figures

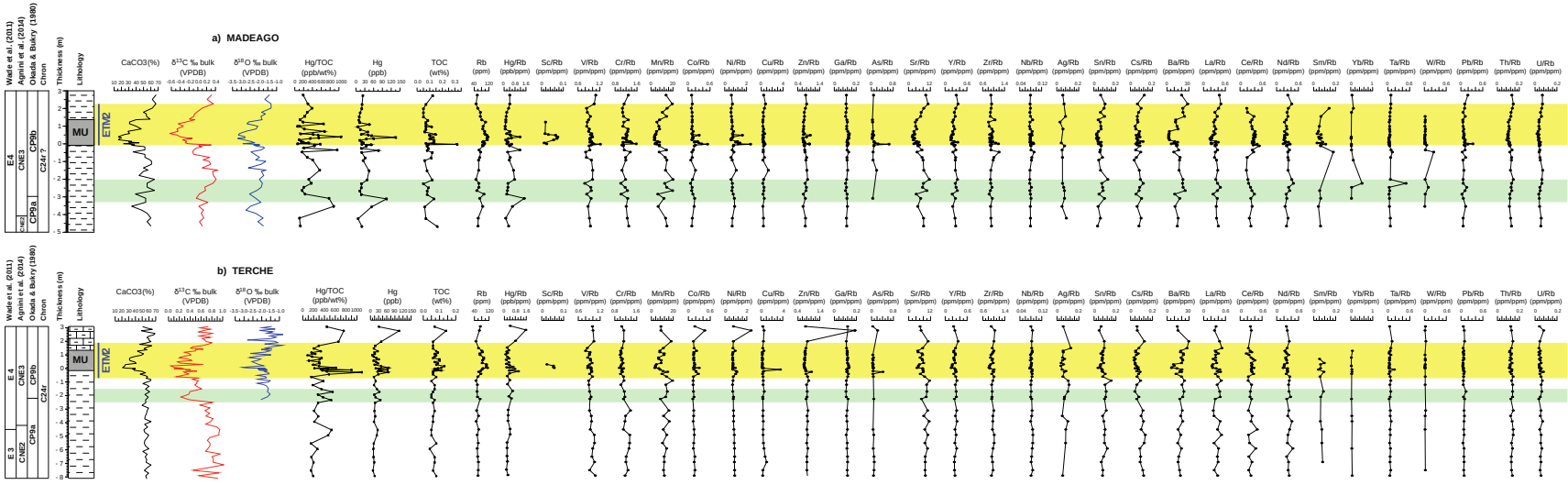

Figure S1. Mercury (Hg) and Total Organic Carbon (TOC) contents and X-ray fluorescence (XRF) trace element concentrations normalized to Rb (a major detrital input tracer) from the Madeago (A) and Terche (B) sections plotted against stratigraphic logs and biostratigraphy. As in the figures from the main text, the yellow and light-green bands highlight the ETM2 interval as defined by the $\delta^{13}C$ shifts and the α CIE interval respectively.

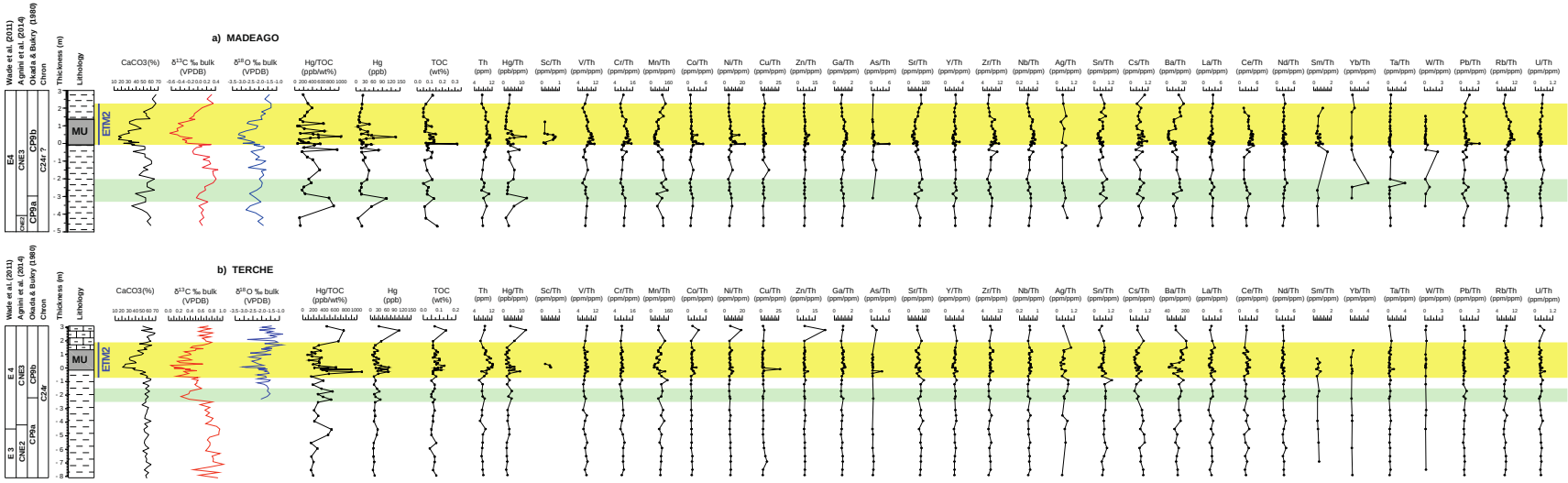

Figure S2. Mercury (Hg) and Total Organic Carbon (TOC) contents and X-ray fluorescence (XRF) trace element concentrations normalized to Th (a major detrital input tracer) from the Madeago (A) and Terche (B) sections plotted against stratigraphic logs and biostratigraphy. As in the figures from the main text, the yellow and light-green bands highlight the ETM2 interval as defined by the $\delta^{13}C$ shifts and the α CIE interval respectively.

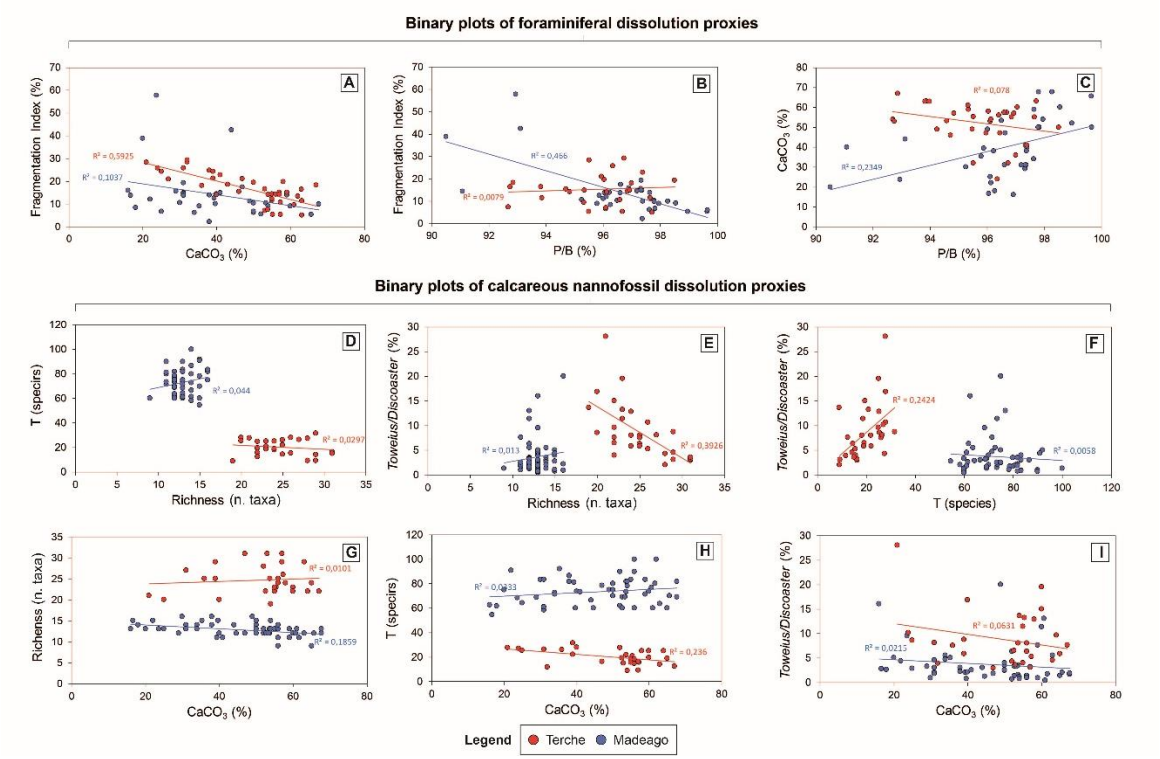

Figure S3. Binary plots of dissolution indices based on foraminifera and calcareous nannofossil count versus each other and the $CaCO_3$ content at the Madeago (in blu) and Terche (in red) sections. Note that, except for a slightly higher correlation $CaCO_3$-Fragmentation index at Terche, both foraminiferal and calcareous dissolution proxies do not show correlation with $CaCO_3$. We do not exclude that the increased dissolution at the ETM2 may have partly amplified abundance and size signals of chiloguembelinid and subbotinids which are particularly prone to dissolution (Nguyen et al., 2009, 2011). However, the low variations recorded by our whole set of dissolution proxies confirm that dissolution at the ETM2 did not significantly impacted the original signal of planktic foraminifera and calcareous nannofossil assemblages.

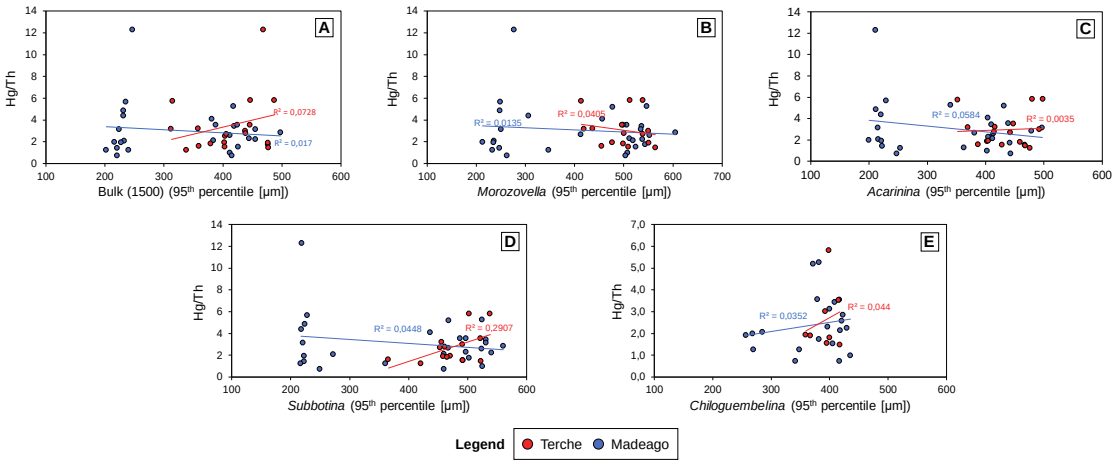

Figure S4. Binary plots of Hg/Th vs planktic foraminiferal assemblages test-size (bulk, 95th percentile, µm) at the Madeago (in blu) and Terche (in red) section (A); Hg/Th vs *Morozovella* (95th percentile, µm) (B); Hg/Th vs *Acarinina* (95th percentile, µm) (C); Hg/Th vs *Subbotina* (95th percentile, µm) (D); Hg/Th vs *Chiloguembelina* (95th percentile, µm) (E). The binary plots do not show correlation between Hg/Th and test-sizes, suggesting no direct but a more indirect link of volcanism and dwarfing despite the peak of mercury in the lower part of the ETM2 interval at both sections. This lack of correlation may derive, at least in part, to the fact that trace metal analysis was performed on a small number of samples. As warming and eutrophication alone cannot explain the recorded striking size reduction we tentatively speculate that the volcanic input of biolimiting/toxic metals could have acted synergistically with these to induce dwarfing and explain the uniqueness of our findings.

3. Titles of data set tables

Datasets for this research are available in .xlsx and html format to the Pangea repository by the DOI of the following dataset publication ***D'Onofrio, et al. (2024): Extreme Planktic Foraminiferal Dwarfism Across the ETM2 in the Tethys Realm in response to warming [dataset bundled publication]. PANGAEA,*** https://doi.org/10.1594/PANGAEA.967574

Table S1. D'Onofrio, R; Barrett, R; Schmidt, DN et al. (2024): Carbonate content, Carbon and Oxygen stable isotopes at the Madeago and Terche sections. https://doi.org/10.1594/PANGAEA.967560

Table S2. D'Onofrio, R; Barrett, R; Schmidt, DN et al. (2024): Total Organic Carbon (TOC) contents and Rock eval Pyrolysis at the Madeago and Terche sections. https://doi.org/10.1594/PANGAEA.967564

Table S3. D'Onofrio, R; Barrett, R; Schmidt, DN et al. (2024): X-ray fluorescence (XRF) trace element concentrations at the Madeago and Terche sections. https://doi.org/10.1594/PANGAEA.967565

Table S4. D'Onofrio, R; Barrett, R; Schmidt, DN et al. (2024): Foraminiferal based dissolution proxies from Madeago and Terche sections. https://doi.org/10.1594/PANGAEA.967566

Table S5. D'Onofrio, R; Barrett, R; Schmidt, DN et al. (2024): Calcareous nannofossil based dissolution proxies from Madeago and Terche sections. https://doi.org/10.1594/PANGAEA.967567

Table S6. D'Onofrio, R; Barrett, R; Schmidt, DN et al. (2024): Planktic foraminifera and Radiolarian abundances at Madeago and Terche sections. https://doi.org/10.1594/PANGAEA.967569

Table S7. D'Onofrio, R; Barrett, R; Schmidt, DN et al. (2024): Planktic foraminifera test-sizes at Madeago and Terche sections. https://doi.org/10.1594/PANGAEA.967570

Table S8. D'Onofrio, R; Barrett, R; Schmidt, DN et al. (2024): Calcareous nannofossil abundances and sizes at Madeago and Terche sections. https://doi.org/10.1594/PANGAEA.967571

Table S9. D'Onofrio, R; Barrett, R; Schmidt, DN et al. (2024): Planktic foraminiferal test-sizes from oceanic ODP Site 198-1209. https://doi.org/10.1594/PANGAEA.967572

Table S10. D'Onofrio, R; Barrett, R; Schmidt, DN et al. (2024): Planktic foraminiferal test-sizes from oceanic ODP Site 208-1263C. https://doi.org/10.1594/PANGAEA.967573